

Charge transfer into excited states of hydrogen atoms reflected on metal surfaces

R. Brako

*Institute for Theoretical Physics, University of California, Santa Barbara, California 93106
and Rudjer Bošković Institute, Bijenička 54, 41001 Zagreb, Croatia, Yugoslavia**

(Received 12 March 1984)

A theory of transfer of electrons into excited states of a proton moving above a free-electron metal surface is presented, based on a time-dependent Anderson Hamiltonian with a degenerate atomic level. The density matrices of the resulting atomic states are calculated. At grazing proton trajectories the parallel velocity effectively brings some of the conduction electrons into resonance with higher atomic levels. This mechanism leads to creation of excited states in which the sublevels within the shell are unsymmetrically populated. The polarization characteristics of Balmer H_α light ($n=3$ to $n=2$ transition) emitted from 9-keV protons scattered at a few degrees are calculated, in good agreement with experimental data. The possible influence upon the electron capture process of the incompleteness of the screening of the fast proton by conduction electrons is discussed.

I. INTRODUCTION

The creation of excited atomic states by transmission of energetic ions through thin foils and by reflection on surfaces has recently been the subject of extensive experimental studies. Such states are usually degenerate or nearly degenerate, and the knowledge of the linear combination into which the electron is captured can provide interesting information about the nature of the atom-solid interaction.

The light emitted during the radiative deexcitation of such states is often linearly or circularly polarized to a high degree, indicating that coherent excited states are produced during the scattering. Several explanations of the mechanism of creation of these states have been proposed, which look for their origin either in the bulk, in the region where the atom leaves the surface, or in the evolution after the initial creation of the excited atom. A brief survey can be found in Ref. 1; yet, no quantitative theory has been developed. We note that the approaches used for charge exchange processes between atoms in the gas phase, where both species have a small number of discrete levels, cannot be applied directly to metal surfaces with delocalized bands.

The aim of this paper is to present a theoretical approach to the problem in which the electronic degrees of freedom are described by a time-dependent Anderson Hamiltonian. This model is already rather simplified (e.g., it neglects the electron-electron interaction from the start), but it has the advantage of being soluble. The results are evidently at least semiquantitative. The experiment we have in mind is the reflection of protons at grazing incidence on a smooth metal surface, such as Ni(110), at energies around 10 keV.¹⁻³ This system offers several advantages from both experimental and theoretical points of view. First, hydrogen atoms do not damage the surface owing to their small mass. Second, the hydrogen atom has no inner-shell excitations which could complicate the process, and its dynamics after leaving the surface is strictly a one-electron problem. The metal surface can be

described by a free-electron jellium model.

The geometry of the experiment and the coordinate frames used are shown in Fig. 1. In Ref. 1 a capacitor was added after the point of scattering with an electric field applied in the direction of the surface normal. The polarization of the light emitted in the direction perpendicular to the scattering plane after a flight of approximately 1 cm from the scattering point was studied as a function of electric field.

We start by making some general remarks about the process. Excited hydrogen states ($n=2,3,\dots$) have rather extended orbitals with expectation values of the radius $\langle r \rangle = [3n^2 - l(l+1)]a_B/2$ ($a_B = \text{Bohr radius}$), and their energies fall within or above the metal conduction band. They therefore cannot exist as well-defined states when the proton is in the bulk or even at the distance of closest approach during the scattering, as the typical interatomic or interelectronic distance in the metal is comparable with or smaller than $\langle r \rangle$. In that region many conduction electrons participate in the screening of the proton. How-

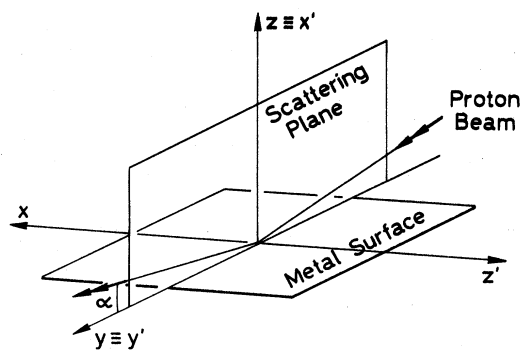


FIG. 1. Geometry of H atom scattering on a metal surface, and the coordinate frames used in the text. In the experiment a capacitor approximately 2 mm long with the electric field in the z direction was placed after the point of scattering. The light emitted in the z' direction was measured, after a flight of approximately 1 cm.

ever, the final atomic state is not simply a projection of this screening charge onto free hydrogen states. A much better picture is that in which the conduction electrons adjust almost adiabatically as the proton recedes from the surface, up to the point where the interaction effectively stops.

These considerations do not apply to the creation of ground-state ($n=1$) atoms, because the energy of the $n=1$ state lies below a typical metal conduction band. Indeed, the latter may be influenced by the electronic wake which exists while the proton is moving inside the metal.^{3,4} As we are only interested in excited states, it will be sufficient to assume that the capture into $n=1$ and $n>1$ is independent, which is quite likely.

In Sec. II the time-dependent electronic Hamiltonian is formulated and solved. In Sec. III the formalism is applied to $n=2$ and $n=3$ hydrogen levels. In Sec. IV the subsequent evolution of the atomic state and the emission of light are treated. Section V contains a discussion of the results.

II. THE HAMILTONIAN AND THE DENSITY MATRIX

We describe the resonant tunneling of electrons between the conduction band of a metal surface and the localized atomic states of a proton using the Anderson model.⁵ In the second quantized form the Hamiltonian reads

$$H = \sum_{\vec{k}} \epsilon_{\vec{k}} n_{\vec{k}} + \sum_{l,m} \epsilon_a(t) n_{lm} + \sum_{\vec{k},l,m} [V_{\vec{k},lm}(t) c_{lm}^\dagger c_{\vec{k}} + \text{H.c.}], \quad (1)$$

where $c_{\vec{k}}^\dagger$ and c_{lm}^\dagger are creation operators for band states $|\vec{k}\rangle$ and atomic states $|l,m\rangle$, respectively, and $n_{\vec{k}} = c_{\vec{k}}^\dagger c_{\vec{k}}$ and $n_{lm} = c_{lm}^\dagger c_{lm}$ are number operators (we use atomic units, $\hbar = m_e = e = 1$). The atomic states are degenerate, and l, m are the usual angular momentum quantum numbers, $l=0,1,2,\dots$, and $-l \leq m \leq l$. The first term describes the conduction electrons, the second the atomic level, and the third is the interaction. We have assumed that the proton moves along a classical trajectory $\vec{r}(t)$, so that the position-dependent energy level $\epsilon_a(\vec{r})$ and tunneling $V_{\vec{k},lm}(\vec{r})$ become time-dependent quantities $\epsilon_a(t)$ and $V_{\vec{k},lm}(t)$, respectively, and we obtain the time-dependent electronic Hamiltonian of Eq. (1).⁶ In fact, it turns out that for calculating the final electronic state of the atom it is sufficient to take into account the outgoing part of the trajectory and assume that the motion is uni-

form, i.e., in cylinder coordinates, $z = v_1 t$, $\vec{\rho} = \vec{v}_\parallel t$.⁷ We have not included the intra-atomic Coulomb repulsion, which is justified when the occupation probability $\sum_{l,m} \langle n_{lm} \rangle$ of the atomic level is small at all times. Then the two spin channels are independent, and Eq. (1) is the Hamiltonian per spin. We have taken only one hydrogen shell (for example, $n=2$ or 3, etc.), assuming that the capture into different shells is uncorrelated. To explain this, we note that the expectation value $\langle r \rangle$ of the orbital radius increases with n^2 . The final electron capture occurs, roughly speaking, when the surface-atomic orbital overlap vanishes as the atom leaves the surface, so that the capture takes place at points far apart in space for different n . The neutralization into $n=1$ (which is somewhat different in nature, because the level lies well below the Fermi level of the metal) occurs first, and only those atoms which are *not* neutralized can subsequently pick up an electron into the $n=2$ state, etc.

The atomic level $\epsilon_a(\vec{r}) = \epsilon_n + \epsilon_{\text{image}}(\vec{r})$ is position dependent because of the image shift near the surface. We have assumed that it is still degenerate with respect to l , since it can be shown that the splitting in the image field is small at the energy scale which is relevant during the capture process. Further on in the paper we shall include the spin-orbit splitting when calculating the evolution of the atomic state after it has left the surface.

Our aim is to calculate the final density matrix ρ at the time $t \rightarrow \infty$. In the Heisenberg representation this is

$$\rho_{lm,l'm'}(t) = \langle t_0 | c_{lm}^\dagger(t) c_{l'm'}(t) | t_0 \rangle, \quad (2)$$

where $|t_0\rangle$ is the electronic state (both metal and atomic) at some time before the interaction. The total capture probability into the level under consideration is $\text{Tr} \rho$, and the degree of coherence is $\text{Tr}(\rho^2)/(\text{Tr} \rho)^2$.

The problem of finding the operator $c(t)$ for Hamiltonians similar to the Hamiltonian of Eq. (1) was first solved by Blandin, Nourtier, and Hone⁸ using the Keldysh formalism. A more usual approach is to work with equations of motion for the operators in the Heisenberg representation.^{9,7} Using Eq. (1) we obtain

$$i\dot{c}_{lm}(t) = -[H, c_{lm}(t)] = \epsilon_a(t) c_{lm}(t) + \sum_{\vec{k}} V_{\vec{k},lm}^*(t) c_{\vec{k}}(t), \quad (3)$$

$$i\dot{c}_{\vec{k}}(t) = -[H, c_{\vec{k}}(t)] = \epsilon_{\vec{k}} c_{\vec{k}}(t) + \sum_{l,m} V_{\vec{k},lm}(t) c_{lm}(t). \quad (4)$$

Equation (4) can be solved and reinserted into Eq. (3), which becomes

$$i\dot{c}_{lm}(t) = \epsilon_a(t) c_{lm}(t) - i \sum_{l',m'} \sum_{\vec{k}} V_{\vec{k},lm}^*(t) \int_{t_0}^t dt' V_{\vec{k},l'm'}(t') c_{l'm'}(t') e^{i\epsilon_{\vec{k}}(t'-t)} + \sum_{\vec{k}} V_{\vec{k},lm}^*(t) c_{\vec{k}}^0 e^{-i\epsilon_{\vec{k}}(t-t_0)}, \quad (5)$$

where $c_{\vec{k}}^0 = c_{\vec{k}}(t_0)$ is the operator at the initial time t_0 .

In order to make further progress, we must make some simplifying assumptions. We assume that the matrix elements $V_{\vec{k},lm}$ factorize as

$$V_{\vec{k},lm}(t) = u(t) V_{\vec{k},lm}. \quad (6)$$

Explicit calculation shows that this is not exactly true, but the time dependence of the overall magnitude is approximately exponential, while the relative importance of dif-

ferent metal states $|\vec{k}\rangle$ varies much more slowly. Equation (6) is then a good approximation taking into account that the final capture of the electron occurs in a rather narrow region of distance z from the surface. We introduce the matrix Δ

$$\Delta_{ll',m}(\epsilon,t) = \pi \sum_{\vec{k}} V_{\vec{k}lm}^*(t) V_{\vec{k},l'm}(t) \delta(\epsilon - \epsilon_{\vec{k}}), \quad (7)$$

which is diagonal in m if the coordinate frame with the z axis perpendicular to the surface is used. We further assume that the energy dependence of V and Δ is small at the energy scale relevant to us. Then the sum over $|\vec{k}\rangle$ in Eq. (5) is proportional to a δ function of $(t-t')$. Making a unitary transformation from the basis $|l,m\rangle$ of atomic states into the basis $|j\rangle$ in which the matrix Δ is diagonal, the differential equation (5) can be integrated to give

$$\begin{aligned} c_j(t) = & -i \int_{t_0}^t dt' \exp \left[\int_{t'}^t d\tau [\Delta_j(\tau) + i\epsilon_a(\tau)] \right] \\ & \times \sum_{\vec{k}} V_{\vec{k},j}^*(t') \\ & \times \exp(-i\epsilon_{\vec{k}} t' + i\epsilon_{\vec{k}+\vec{Q}} t_0) c_{\vec{k}+\vec{Q}}^0. \end{aligned} \quad (8)$$

Here we have omitted a term proportional to c_{lm}^0 , because it would produce effects due to the "memory" of the initial atomic state. These effects are negligible in the situation considered here.⁷ We have assumed that the surface is completely translationally invariant and we use the coordinate frame which follows the adatom motion parallel to the surface. The parallel motion has the effect of translating in \vec{k} space the fermion operator by $Q = (\vec{Q}, 0)$, $\vec{Q} = \vec{v}_{\parallel}$.¹⁰ The density matrix of Eq. (2) at $t \rightarrow \infty$ is found to be

$$\rho_{ij} = \sum_{\vec{k}} F_i(\epsilon_{\vec{k}}) F_j^*(\epsilon_{\vec{k}}) V_{\vec{k},i} V_{\vec{k},j}^* f_{\vec{k}+\vec{Q}}, \quad (9)$$

where the function F is

$$F_i(\epsilon) = \int_{t_0}^{\infty} dt u(t) \exp \left[\int_{\infty}^t dt' [\Delta_i u^2(t') + i\epsilon_a(t')] - i\epsilon t \right] \quad (10)$$

and where $f_{\vec{k}+\vec{Q}} = \langle c_{\vec{k}+\vec{Q}}^{\dagger} c_{\vec{k}+\vec{Q}}^0 \rangle$ is the Fermi distribution. (The time dependence of V and Δ according to Eq. (6) has been explicitly written down.) Equations (9) and (10) can be evaluated numerically for a specific form of $u(t)$ and $\epsilon_a(t)$. Instead of doing that, we make further approximations. The functions $u(t)$ and $\epsilon_a(t)$ are smooth. For $t \rightarrow \infty$, $u(t)$ vanishes and $u(t_0)$ is very large. The integrand in Eq. (10) is therefore non-negligible only in a narrow interval of t , delimited on the one side by the vanishingly small $u(t)$ and on the other side by the exponential of the integral of $[u(t)]^2$. Let us denote t^* a value from this interval and $z^* = v_{\parallel} t^*$ the corresponding distance. The integral $F(\epsilon)$ itself will be peaked around some energy $\epsilon^* \approx \epsilon_a(t^*)$, the width of the peak becoming smaller for $v_{\parallel} \rightarrow 0$. The velocity v_{\parallel} in Ref. 1 is sufficient-

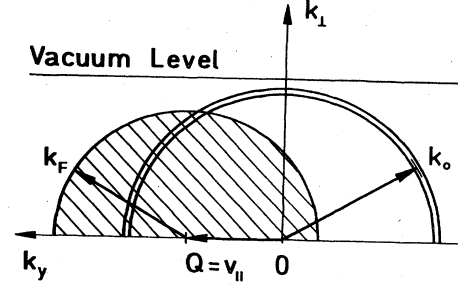


FIG. 2. Factors in Eq. (9), in \vec{k} space. The spherical shell at energy $\epsilon^* = \frac{1}{2}k_0^2$ is the factor $F_i F_j^*$, the shaded area is the translated Fermi sphere $f_{\vec{k}+\vec{Q}}$. Owing to the factor $V_{\vec{k},i} V_{\vec{k},j}^*$ the only significant contribution to the density matrix ρ comes from the region where the spherical shell just starts to intersect the Fermi sphere.

ly small to make this peak very narrow compared with, for example, ϵ_F . Figure 2 shows the spherical shell in k space corresponding to the maximum of $F_i F_j^*$, together with the translated Fermi sphere $f_{\vec{k}+\vec{Q}}$. The third factor in Eq. (9), $V_{\vec{k},i} V_{\vec{k},j}^*$, depends only upon the "angular" coordinates of \vec{k} , and has its maximum for \vec{k} vectors perpendicular to the surface. The velocity of 9-keV protons is comparable with v_F of typical metals, and therefore higher hydrogen levels, which for an atom at rest lie above the Fermi level of the metal (remember that an upward image energy shift exists near the surface), now intersect the translated Fermi sphere. This situation is similar to the finite-temperature case discussed in Ref. 7, although the origin of the partial overlap of ϵ^* with occupied states is different: In Ref. 7 it was the tail of high-temperature Fermi distribution, and here it is the motion of the atom parallel to the surface. The approximation consists in neglecting the width of the maximum of Eq. (10) altogether and approximating it by a δ function. It can be easily proved that

$$\sum_{\vec{k}} F_i F_j^* V_{\vec{k},i} V_{\vec{k},j}^* = \delta_{ij} \quad (11)$$

by using the assumed energy independence of $V_{\vec{k},i} V_{\vec{k},j}^*$ and writing the sum over k states as an energy integral and two angular integrals. Therefore, approximately

$$F_i(\epsilon) F_j^*(\epsilon) = \frac{2\pi}{\Delta_i + \Delta_j} \delta(\epsilon - \epsilon^*), \quad (12)$$

so that the density matrix of Eq. (9) becomes

$$\rho_{ij} = \sum_{\vec{k}} \frac{2\pi}{\Delta_i + \Delta_j} V_{\vec{k},i} V_{\vec{k},j}^* f_{\vec{k}+\vec{Q}} \delta(\epsilon_{\vec{k}} - \epsilon^*). \quad (13)$$

This expression can be evaluated if the matrix elements V are known. Once calculated, the density matrix can be transformed back into the familiar $|l,m\rangle$ basis.

III. APPLICATION TO HYDROGEN ATOM STATES

To calculate the matrix elements occurring in the density matrix of Eq. (13), we have employed the usual approximation

$$V_{\vec{k},lm}(z) = \langle \vec{k} | V | l, m \rangle, \quad (14)$$

where $V=1/r$ is the Coulomb potential of a proton at distance z from the surface, $|l, m\rangle$ are the atomic states of the shell under consideration, and $|k\rangle$ are the unperturbed metal states.

Grozdanov and Janev¹¹ have found the matrix Δ , Eq. (7), for a hydrogenic atom by using a nonperturbative method. In their approach, Δ is diagonal in the basis of Stark states.¹² However, we need more information; namely, we also need the dependence of the matrix elements upon the angular variables which are integrated over when calculating Δ , so that the results of Grozdanov and Janev can only serve as a check.

Figure 3 shows the potential energy of the proton-surface system along the surface normal. The "relevant" distance z^* lies where $|l, m\rangle$ states overlap with the very tail of $|k\rangle$ states. This tail is determined solely by the electron self-image

$$V(z) = -1/4z, \quad (15)$$

where $z=0$ has been put at the image plane. An approximate solution of Eq. (15) is

$$C_{\vec{k}} z^{1/4} \exp(-qz + i\vec{k}_{\parallel} \cdot \vec{\rho}), \quad (16)$$

where $q = (2\epsilon + k_{\parallel}^2)^{1/2}$ and ϵ is the energy measured from the vacuum level. On the other hand, the potential in the bulk is constant:

$$V(z) = -V_0. \quad (17)$$

In principle, Eqs. (15) and (17) should be joined smoothly by a realistic surface potential and the normalization con-

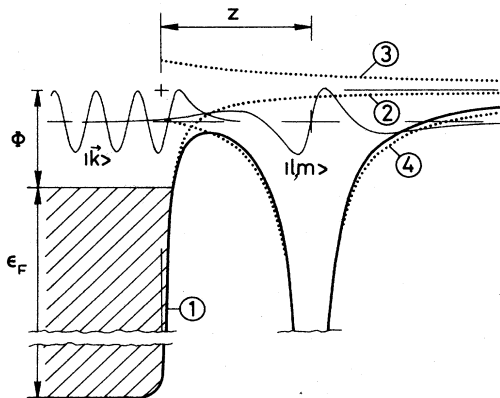


FIG. 3. Various contributions to the atom-surface potential, schematically: surface potential, 1; electron image, 2; core image, 3; Coulomb potential of the proton, 4. Also shown are a metal electron wave function $|k\rangle$ (an eigenfunction of 1 and 2) and an atom wave function $|l, m\rangle$ (an eigenfunction of 4). To a good approximation, potentials 2 and 3 only shift the local vacuum level, i.e., Φ .

stants $C_{\vec{k}}$ in Eq. (16) found accordingly. The *strong* \vec{k}_{\parallel} dependence of the matrix elements of Eq. (14) comes from the factor $\exp(i\vec{k}_{\parallel} \cdot \vec{\rho})$ in Eq. (16), which at large k_{\parallel} oscillates rapidly and makes the integral small. The normalization constants $C_{\vec{k}}$ have a weaker k_{\parallel} dependence in any case, and their absolute value is unimportant to us. Therefore we do not make a serious error if we use a surface potential with a discontinuous jump from Eq. (15) to Eq. (17) at some $z > 0$, which makes it possible to calculate the constants $C_{\vec{k}}$ analytically. Some details of the evaluation of the matrix elements of Eq. (14), using the wave functions of Eq. (16), are given in the Appendix. The calculated $\Delta(z)$, Eq. (7), agrees well with the analytic formula of Ref. 11, although the basis in which it is diagonal is only close to, but not identical with, the Stark basis.¹³

Finally, we must determine the distance z^* , as discussed after Eq. (10). Here we encounter a difficulty, because various elements of the diagonalized Δ differ by orders of magnitude for the same value of z , and therefore give different z^* . In the calculations we have used an "average" z^* , an approximation which will be justified *a posteriori*. Also, the factorization of Eq. (6) does not hold exactly, the half-width in k_{\parallel} of $V_{\vec{k},lm}(z)$ becoming smaller at larger z . We have used $V_{\vec{k},lm}(z^*)$. For 9-keV protons reflected at an angle of 5° with respect to the surface, the estimate is $z^* = 9$ a.u. for $n=2$ and $z^* = 20$ a.u. for $n=3$.

To recapitulate, the perpendicular velocity v_{\perp} of the atom enters into the final result only through z^* , which in turn specifies $V_{\vec{k},lm}(z^*)$ and the image shift of the level $\epsilon_{\text{image}}(z^*)$. The parallel velocity v_{\parallel} enters into Eq. (13) through the translated Fermi sphere.

The only symmetry element of the whole system is the scattering plane, and the atomic states are either even or odd with respect to it. The off-diagonal elements of the density matrix between states of different parity are zero. In fact, the population of odd states is very small, only about 2% of the total in the $n=3$ case and 4.5% in the $n=2$ case. The states with positive m (the z' axis perpendicular to the scattering plane) are preferentially populated over those with negative m .

For $n=3$, $z^* = 20$ a.u., and $\Phi = 4.6$ eV, the calculated total capture probability is $\text{Tr}\rho = 0.0013$. This value should be interpreted as the probability of neutralization into the $n=3$ state of those atoms which have not previously been neutralized into $n=1$ or $n=2$. There is no experimental data for comparison, but this value is reasonable. The density matrix is quite coherent, with $\text{Tr}(\rho^2)/(\text{Tr}\rho)^2 = 0.57$. (This quantity can vary from $\frac{1}{9}$ for equally probable incoherent occupation of each of the 9 sublevels to 1 for a completely coherent state.) The best single-function representation of the even and odd part of the normalized density matrix $\rho/(\text{Tr}\rho)$ is

$$\begin{aligned} |e\rangle &= 0.496 |s,0\rangle + 0.377 |p,-1\rangle - 0.576 |p,1\rangle \\ &\quad + 0.203 |d,-2\rangle - 0.152 |d,0\rangle + 0.442 |d,2\rangle, \\ |o\rangle &= 0.091 |p,0\rangle + 0.047 |d,-1\rangle - 0.101 |d,1\rangle. \end{aligned} \quad (18)$$

Incomplete coherence means that the off-diagonal elements of the true density matrix are smaller than those resulting from Eq. (18).

The value of the work function Φ of the metal influences the *total* capture probability more strongly than the relative amplitudes, i.e., the normalized density matrix. This dependence is still much weaker than in the case of small parallel velocity. For example, even the case when the adatom level is below ϵ_F (i.e., the Fermi sphere in Fig. 2 larger than k_0) is only quantitatively different at large velocity, while for small v_{\parallel} it would be qualitatively different, giving $n_a \approx 1$.

The capture probability varies strongly if we choose another value of z^* ; thus for $n=3$ and $z^*=30$ a.u., it is 0.00002, while the coherence increases slightly to 0.63. On the other hand, the normalized density matrix changes very little. This is the main argument in support of choosing a single z^* , as the polarization of the emitted light depends only upon the relative magnitude of the elements of ρ .

Some caution is still necessary, because the large difference between the elements of Δ may lead to a somewhat different density matrix if a more complete theory (i.e., not assuming a single z^*) is used. Still, the diagonal element which is largest when using Eq. (13) will remain largest, etc., and the phase of the off-diagonal elements will not be substantially altered.

For $n=2$ and $z^*=9$ a.u., the capture probability is 0.12 and the coherence is 0.56. The relative population of odd states is larger and the coherence of the density matrix is smaller than for $n=3$, which means that the capture from a larger number of states can occur. The best single-function representation is

$$\begin{aligned} |e\rangle &= 0.552 |s, 0\rangle + 0.344 |p, -1\rangle - 0.729 |p, 1\rangle, \\ |o\rangle &= 0.212 |p, 0\rangle. \end{aligned} \quad (19)$$

Finally, we discuss another effect which possibly influences the final density matrix. It has been observed that the axes of the elliptically polarized Balmer α light ($n=3$ to $n=2$ transition) appearing along the z' direction are not respectively parallel and perpendicular to the surface, but lie obliquely.¹ Density matrices with real coefficients, such as the one defined by Eq. (18), cannot explain this feature. The evolution in surface electric field of the excited state *after* its creation has sometimes been invoked,¹⁴ and here we examine this possibility in some detail.

The obvious question is what the nature of the additional electric field is like. Near a metal surface any free charge is rapidly screened by conduction electrons, so that long-range electric fields are improbable. After the capture, the excited atom is a neutral object. Still, the different nature of the image potential of the proton and the self-image of the electron has two consequences. First, the difference between them at the site of the proton gives an upward shift of the level (which we have included). Second, their different spatial dependence *around* the proton can be regarded as an additional perturbing potential. However, in the first-order perturbation calculation this potential does not split the degenerate hydrogen levels. Higher-order effects cannot cause an appreciable phase

evolution of the density matrix.

This discussion has assumed that the charge screening is perfect. In fact, the velocity of a 9-keV proton is comparable with the Fermi velocity of metal electrons, and the charge screening a proton which moves parallel to the surface is not fast enough to follow it, but lags behind it. This surface wake has been studied in detail, mostly in connection with energy loss to surface plasmons of fast ions.¹⁵ The parallel component of the force (and therefore of the field at the site of the proton) is¹⁵

$$F_{\parallel} = \frac{1}{2} \left[\frac{\omega_s}{v_{\parallel}} \right]^2 K_0 \left[\frac{2\omega_s z}{v_{\parallel}} \right], \quad (20)$$

where ω_s is the surface plasmon frequency. A local Drude dielectric response of the metal has been assumed. This approach can be easily generalized to calculate the field at other points in space, and it turns out that it is not very different from Eq. (20) in the whole region between the proton and the metal. The Bessel function K_0 decreases rapidly with increasing z , so that the effect is restricted to a region very close to the surface. In other words, the screening of a charge moving parallel to the surface at larger distances becomes perfect quickly. If, however, a larger imaginary part of the dielectric function is assumed, the effect has a longer range, decreasing as z^{-3} .¹⁶

We have restricted our attention only to the parallel component of the field. This component does not exist with perfect screening and it alters the symmetry of the atom-metal interaction. It seems that it is more likely that the effect influences the capture process itself, and not the subsequent evolution of the already created state. It is difficult to estimate the value of F_{\parallel} quantitatively, as the dielectric function of Ni, which was used in the experiment,^{1,2} cannot be approximated well with the Drude function, and it is even more difficult to calculate the matrix elements of Eq. (14) with the complicated field due to the wake effect. The simplest approximation is to add a *constant* electric field parallel to the surface to the potential V in Eq. (14). Then the matrix elements can still be calculated by the method described in the Appendix. We have done this for $n=2$. Qualitatively, the result is that the coefficients in Eq. (19) become complex, as if a rotation by a small angle around the z' axis (Fig. 1) were performed. This agrees with the qualitative picture that the tunneling on the front side of the proton where there is less accumulated image charge is preferred, and also with the experiment (see next section). However, it would be premature to draw definite conclusions, as the effect has not been estimated quantitatively.

IV. TIME EVOLUTION AND RADIATION DEEXCITATION OF ATOMIC STATES

The interaction of the atom with the surface stops at several tens of angstroms at the most. After that the atomic state evolves under the free-atom Hamiltonian. Owing to comparatively long times of flight (the distance between the surface and the spectrometer slit in Ref. 1 is approximately 1 cm), a new, much finer energy scale be-

comes important. This includes the spin-orbit and Lamb shift splittings of the sublevels, the width due to radiative transitions to lower states, and, if an external electric field is applied along a part of the trajectory,^{1,2} the Stark splitting. The first step is to construct the initial density matrix, including spin. We assume that the capture into each spin state is equal and independent, so that the density matrix consists of two submatrices as found in the preceding section, in the basis which is a direct product of the orbital and the spin basis. Thus the matrix is of order 8 when $n=2$ and 18 when $n=3$. This can now be transformed into the $|nlj\mu\rangle$ basis in which the spin-orbit and Lamb splittings are diagonal:

$$|n,l,j,\mu\rangle = \sum_{m,s} \langle l,m,\frac{1}{2},s | j,\mu \rangle |n,l,m\rangle |s\rangle. \quad (21)$$

Here $\langle l,m,\frac{1}{2},s | j,\mu \rangle$ are Clebsch-Gordan coefficients and $s = \pm \frac{1}{2}$ is the spin index. A convenient approximate description of the time evolution of the density matrix is the so-called Bethe-Lamb approach, based on the effective non-Hermitian Hamiltonian

$$H_{\text{eff}} = H_0 - \frac{i}{2}\Gamma, \quad (22)$$

where H_0 contains the energy splitting and Γ is the width due to the radiative decay. The equation of motion for the density matrix is

$$\frac{d\rho}{dt} = -i[H_0, \rho] - \frac{1}{2}\{\Gamma, \rho\}, \quad (23)$$

where the square brackets and the curly brackets denote a commutator and an anticommutator, respectively.

If the Hamiltonian of Eq. (22) is time independent, i.e., with no field or with a constant external field, it can be diagonalized by a nonunitary matrix S , giving complex eigenvalues λ_n . Then the solution of Eq. (23) can be written as

$$\rho(t) = S \{ e^{-i(\lambda_m - \lambda_n^*)t} [S^{-1}\rho(0)(S^\dagger)^{-1}]_{mn} \} S^\dagger, \quad (24)$$

where $\rho(0)$ is the initial ($t=0$) density matrix. If the Hamiltonian (22) is explicitly time dependent, Eq. (23) must be integrated numerically.

In our calculations we have used the solution in Eq. (24), assuming that the atom first traverses a region without field, then a region with a constant electric field, and finally another field-free region. This is, of course, a rather simplified description of the experiment in Ref. 1 where the condenser plates are approximately 2 mm long and 3 mm apart, and consequently the electric field is quite inhomogeneous. However, the Stark effect of hydrogen is linear, and this description will on average give correct phase evolution, although we cannot hope to reproduce all the details of the field dependence of Stokes parameters. The fine-structure splitting and the decay widths of hydrogen $n=2$ and $n=3$ levels are given in Table I.¹⁷ The $2s$ level is metastable, having no allowed electric dipole transition. The decay width of $3p$ levels consists of transitions to $2s$ and to $1s$; the latter was not measured in Ref. 1. The Stark splitting is¹²

$$E = \frac{3}{2} \mathcal{E} n(n_1 - n_2), \quad (25)$$

TABLE I. The fine-structure splitting ΔE (relative to the lowest sublevels) and the electric-dipole transition widths Γ for $n=2$ and $n=3$ states of hydrogen atoms.

nl	Γ (10^{-9} a.u.)	j	ΔE (10^{-7} a.u.)
$2s$	0	$\frac{1}{2}$	1.6
$2p$	15	$\frac{1}{2}$	0
		$\frac{3}{2}$	16.6
$3s$	0.15	$\frac{1}{2}$	0.5
$3p$	4.6	$\frac{1}{2}$	0
		$\frac{3}{2}$	4.9
		$\frac{5}{2}$	4.9
$3d$	1.6	$\frac{3}{2}$	4.9
		$\frac{5}{2}$	6.5

where \mathcal{E} is the electric field, n is the principal quantum number, and n_1, n_2 are parabolic quantum numbers, $n = n_1 + n_2 + |m| + 1$.

The steps of the calculation of the evolution of the density matrix and the polarization of the emitted light can be summarized as follows.

- (1) Form the initial density matrix, including spin.
- (2) Form the Hamiltonian of Eq. (22) without external field, diagonalize it to find S and λ_n , use Eq. (24) to find the density matrix after the first part of the trajectory. We have included some averaging over time to account for the spread of atom velocities, points of creation, etc.
- (3) Repeat (2) for the part of the trajectory inside the condenser, including field.
- (4) Repeat (2) for the last part of the trajectory, without field.
- (5) Use the density matrix obtained to calculate the properties of the emitted light.

The polarization of the light is usually expressed through the Stokes parameters

$$\begin{aligned} \frac{S}{I} &= \frac{I_{\text{RHC}} - I_{\text{LHC}}}{I_{\text{RHC}} + I_{\text{LHC}}}, \\ \frac{M}{I} &= \frac{I_{0^\circ} - I_{90^\circ}}{I_{0^\circ} + I_{90^\circ}}, \\ \frac{C}{I} &= \frac{I_{45^\circ} - I_{135^\circ}}{I_{45^\circ} + I_{135^\circ}}. \end{aligned} \quad (26)$$

Here I_{0° , I_{45° , I_{90° , and I_{135° are the intensities of linearly polarized light emitted along the z' direction. The number denotes the polarization plane, 0° being along the surface normal and 90° along $\vec{v}_{||}$. I_{RHC} and I_{LHC} are the intensities of light with right-hand and left-hand circular polarizations, respectively.

Figure 4 shows the calculated Stokes parameters for $n=3$, with an applied electric field from -800 to $+800$ V/cm. Comparison with experimental data¹ shows good agreement for the position of oscillations. The general shape of the curves is also well reproduced, although some finer details are not. However, in the experiment, C/I is

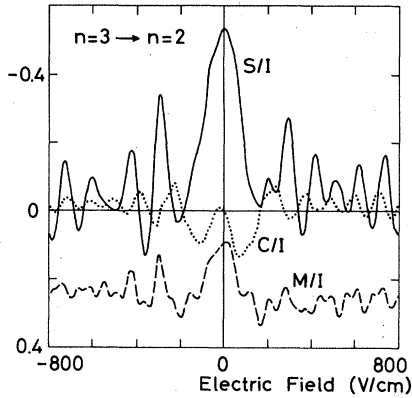


FIG. 4. Calculated Stokes parameters of light emitted in the $n=3$ to $n=2$ transition as a function of applied electric field.

not zero at zero field. An explanation of this discrepancy was proposed at the end of the preceding section.

Figure 5 shows the results for $n=2$. The curves are now symmetric with respect to the sign of the electric field. This is due to the simpler structure of $n=2$ states, for which the eigenstates of the effective Hamiltonian and hence the time evolution is symmetric with respect to the field. There are no experimental data for direct comparison of these calculations, because the linear and especially the circular polarization of the corresponding uv light are difficult to measure.

V. DISCUSSION

The theory presented in this paper gives a clear physical picture of the process of electron capture into excited hydrogen states ($n=2,3,\dots$) during the scattering of protons on a metal surface. When the proton is close to the first layer of atoms (and the point of reflection of grazing incident protons is certainly in this region), it acts as a scattering center for metal conduction electrons, but no sufficiently stable resonance states can be formed. As the proton moves away from the surface, hydrogen atom states appear as resonances. The motion of the atom parallel to the surface is crucial because it enables some of the metal electrons to match the energy of hydrogen orbi-

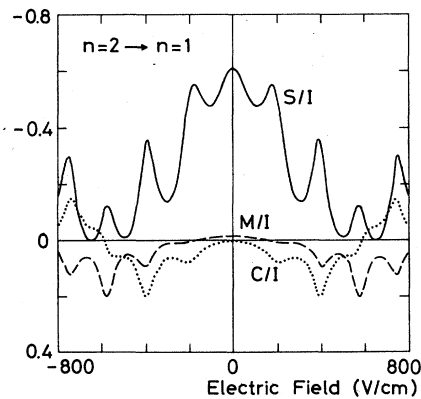


FIG. 5. Same as Fig. 4, but for the $n=2$ to $n=1$ transition.

tals. Thus the resonances have a small average occupation due to continuous population from occupied metal states and depopulation into empty states. The final state reflects the situation at the point where the tunneling finally becomes too slow and the atom-metal interaction effectively stops.

The general agreement of calculated curves with experimental data is very good. One may ask if better agreement in details would be obtained by using Eqs. (9) and (10) instead of the approximation of Eq. (13), and calculating the matrix elements of Eq. (14) with better wave functions. However, one must keep in mind that the Hamiltonian of Eq. (1) and the density matrix of Eq. (9) are already approximations, so that complete quantitative agreement cannot be expected.

Another approximation is that we have assumed free metal electrons, in particular, not including any surface periodicity. The optimum resonance condition (see Fig. 2) occurs when the parallel velocity of the atom is $\sim |2(\epsilon_a - \epsilon_F)|^{1/2}$. For a typical metal work function this corresponds to protons with kinetic energies of 3 and 7 keV for $n=2$ and $n=3$ states, respectively. This mechanism exists up to a proton velocity of $\sim 2v_F$, i.e., a kinetic energy of 100 keV. At higher proton energies the resonance condition according to Eq. (13) cannot be achieved, and a more complete model must be used, probably with the atomic structure of the surface included.

The capture is a purely surface process, but it depends on the very tail of the metal electron density, which has a universal form for all smooth metal surfaces (to within a normalization constant). Therefore the normalized density matrix of the final state, and hence the polarization of the emitted light, is not expected to be surface specific.

ACKNOWLEDGMENTS

I am grateful to W. Kohn and members of the Institute for Theoretical Physics at Santa Barbara. I would like to thank D. M. Newns and N. H. Tolk for discussions, and J. C. Tully for his help with computing the Stokes parameters. This research was supported in part by the National Science Foundation Grant No. PHY-77-27084.

APPENDIX

With use of Eq. (16), the matrix element (14) becomes

$$V_{\vec{k},lm}(z_0) = C_{\vec{k}} \int_0^\infty dz z^{1/4} e^{-qz} I_{nlm}(z_0, z), \quad (\text{A1})$$

where

$$I_{nlm}(z_0, z) = \int_{-\infty}^\infty dx \int_{-\infty}^\infty dy e^{ik_{||}(x \cos\phi + y \sin\phi)} \times V(\vec{r}) \psi_{nlm}(\vec{r}). \quad (\text{A2})$$

Here ϕ is the angle between the x axis and $k_{||}$, $V(r)$ is the Coulomb potential centered around z_0 :

$$V = r^{-1} = [x^2 + y^2 + (z - z_0)^2]^{-1/2}, \quad (\text{A3})$$

and ψ are hydrogen-atom wave functions around the same point. Using the real representation of spherical harmonics,¹⁸ we can write

$$\psi_{nlm}^i = Ne^{-r/n} P(x, y, z, r), \quad (\text{A4})$$

where the value of the index i may be even (e) or odd (o), $0 \leq m \leq l$, and P is a polynomial. The integrals (A2) can be found from the basic integral

$$\begin{aligned} I &= \int_{-\infty}^{\infty} dx \int_{-\infty}^{\infty} dy r^{-1} e^{iax + iby - cr} \\ &= 2\pi(a^2 + b^2 + c^2)^{-1/2} \\ &\quad \times \exp[-|z - z_0|(a^2 + b^2 + c^2)^{1/2}] \end{aligned} \quad (\text{A5})$$

by taking the derivatives with respect to a , b , and c . As

an example, for $n = 2$, $l = 1$, $m = 1$, and i even,

$$\psi_{211}^e = (32\pi)^{-1/2} x e^{-r/2} \quad (\text{A6})$$

and

$$I_{211}^e = \left(\frac{1}{8}\pi\right)^{1/2} i q^{-3} k_{\parallel} \cos\phi e^{-q|z-z_0|} (1 + q|z-z_0|), \quad (\text{A7})$$

where $q = (2\epsilon_2 + k_{\parallel}^2)^{1/2}$. The integral over z in Eq. (A1) must be performed numerically.

*Permanent address.

- ¹J. C. Tully, N. H. Tolk, J. S. Kraus, C. Rau, and R. Morris, in *Inelastic Particle-Surface Collisions*, edited by W. Heiland and E. Taglauer (Springer, Berlin, 1981), pp. 196–206.
- ²N. H. Tolk, J. C. Tully, and Y. Niv, in *Physics of Electronic and Atomic Collisions*, edited by S. Datz (North-Holland, Amsterdam, 1982), pp. 833–840.
- ³N. H. Tolk, J. C. Tully, L. C. Feldman, J. S. Kraus, Y. Niv, G. M. Temmer, and M. Hass, *Nucl. Instrum. Methods* **202**, 247 (1982).
- ⁴F. Guinea, F. Flores, and P. M. Echenique, *Phys. Rev. B* **25**, 6109 (1982); A. Mazzaro, P. M. Echenique, and R. H. Ritchie, *ibid.* **27**, 4117 (1983).
- ⁵P. W. Anderson, *Phys. Rev.* **124**, 41 (1961); D. M. Newns, *ibid.* **178**, 1123 (1969).
- ⁶A number of applications of this kind of Hamiltonian to surface problems are given in R. Brako and D. M. Newns, *Vacuum* **32**, 39 (1982).
- ⁷R. Brako and D. M. Newns, *Surf. Sci.* **108**, 253 (1981).

- ⁸A. Blandin, A. Nourtier, and D. Hone, *J. Phys. (Paris)* **37**, 369 (1976); A. Nourtier, Thèse d'Etat, Orsay, Université de Paris-Sud (1976).
- ⁹W. Bloss and D. Hone, *Surf. Sci.* **72**, 277 (1978).
- ¹⁰J. N. M. Van Wunnik, R. Brako, K. Makoshi, and D. M. Newns, *Surf. Sci.* **126**, 618 (1983).
- ¹¹T. P. Grozdanov and R. K. Janev, *J. Phys. B* **10**, 1385 (1977).
- ¹²L. D. Landau and E. M. Lifshitz, *Quantum Mechanics: Non-Relativistic Theory* (Pergamon, New York, 1977).
- ¹³For nonhydrogenic systems, where states are not degenerate in l , the matrix Δ would be diagonal in the $|l, m\rangle$ basis.
- ¹⁴See also the discussion in J. Burgdörfer, *Nucl. Instrum. Methods* **202**, 253 (1982).
- ¹⁵J. P. Muscat and D. M. Newns, *Surf. Sci.* **64**, 641 (1977).
- ¹⁶R. Núñez, P. M. Echenique, and R. H. Ritchie, *J. Phys. C* **13**, 4229 (1980).
- ¹⁷K. Omidvar, *At. Data Nucl. Data Tables* **28**, 1 (1983).
- ¹⁸P. M. Morse and H. Feshbach, *Methods of Theoretical Physics* (McGraw-Hill, New York, 1953), part 2.